Rare Metal Materials and Engineering
Volume 55, Issue 9, September 2026
Available online at www.rmme.ac.cn

Science Press

Cite this article as: Li Chunyan, Liu Jianhui, Gao Jiaqing, et al. Annealing-Induced Enhancement in Mechanical Strength and Corrosion Resistance of Spark-Plasma-Sintered Fe-Based Bulk Metallic Glasses[J]. Rare Metal Materials and Engineering, 2026, 55(09): 2133-2141. DOI: https://doi.org/10.12442/j.issn.1002-185X.20250481.

ARTICLE

Annealing-Induced Enhancement in Mechanical Strength and Corrosion Resistance of Spark-Plasma-Sintered Fe-Based Bulk Metallic Glasses

Li Chunyan[1,2,3], Liu Jianhui[2], Gao Jiaqing[2], Chen Jiaxin[2], Quan Guoning[2], Zhang Qiang[2], Kou Shengzhong[1,2,3], Li Xiaocheng[1,2]

[1] State Key Laboratory of Advanced Processing and Recycling of Nonferrous Metals, Lanzhou University of Technology, Lanzhou 730050, China; [2] School of Materials Science and Engineering, Lanzhou University of Technology, Lanzhou 730050, China; [3] Wenzhou Engineering Institute of Pump & Valve, Lanzhou University of Technology, Wenzhou 325105, China

Abstract: FeCrMoBC bulk metallic glasses (BMGs) were synthesized via spark plasma sintering (SPS) technique, and subsequent heat treatment was applied to optimize their properties. The effects of annealing on the microstructure, mechanical behavior, and corrosion resistance of the Fe-based BMGs were investigated. Results show that under optimized SPS parameters (sintering temperature of 560 °C, consolidation pressure of 550 MPa, and holding time of 1 min), the as-sintered sample achieves a relative density of 94.40% and a compressive strength of 678 MPa. After heat treatment at 550 °C for 20 min, an amorphous matrix with enhanced mechanical properties can be obtained: the compressive strength increases to 884 MPa, accompanied by superior corrosion resistance, which is characterized by corrosion potential (E_{corr}) of −0.318 V, corrosion current density (I_{corr}) of 2.098×10^{-7} A/cm^2, and polarization resistance (R_2) of 59 379 Ω·cm^2. Notably, annealing at 650 °C for 20 min results in a maximum relative density of 97.23% and a peak microhardness of 758.86 HV, which is attributed to the crystalline phase precipitation and grain refinement. These results demonstrate that controlled heat treatment can effectively improve the densification and comprehensive properties of SPS-processed Fe-based BMGs by regulating the microstructure evolution.

Key words: SPS technique; Fe-based BMG; heat treatment; mechanical behavior; corrosion resistance

1 Introduction

Bulk metallic glasses (BMGs), characterized by their unique non-crystalline atomic structure featuring long-range disorder and short-range order, possess exceptional properties, including high strength, excellent elastic modulus, superior soft magnetic performance, and outstanding corrosion resistance[1–7]. These advantages render them promising candidates for advanced applications in functional devices and structural engineering[8–12]. Among various BMG systems, Fe-based BMGs have emerged as desirable materials for structural applications due to their cost-effectiveness and inherent corrosion resistance. Notably, the practical implementation of Fe-based BMGs is severely restricted by their glass-forming ability, which restricts the fabrication of bulk amorphous components via conventional copper mold suction casting to critical sizes below 3 mm[13–15]. This size restriction significantly hinders the applications in engineering fields, necessitating the development of alternative processing methods to overcome this bottleneck.

Spark plasma sintering (SPS), as a rapid and efficient powder metallurgy technique, achieves densification of amorphous powders within a short time by activating particle interfaces and inducing rapid heating via pulsed currents, which is suitable for fabricating BMGs[16–21]. Although SPS effectively preserves the amorphous structure, high-

Received date: September 21, 2025
Foundation item: National Natural Science Foundation of China (52261032, 51861021); Science and Technology Plan of Gansu Province (21YF5GA074); Public Welfare Project of Zhejiang Natural Science Foundation (LGG22E010008); Wenzhou Basic Public Welfare Scientific Research Project (G2023020)
Corresponding author: Li Chunyan, Ph. D., Professor, State Key Laboratory of Advanced Processing and Recycling of Nonferrous Metals, Lanzhou University of Technology, Lanzhou 730050, P. R. China, E-mail: lichunyan@lut.edu.com

temperature processing time and slow cooling rates during sintering may still cause local crystallization, compromising the uniformity of material properties. Annealing treatment, a critical method for controlling the microstructure of amorphous alloys, can optimize mechanical properties by inducing atomic relaxation or nanocrystallization through precise control of annealing temperature and duration[22–27]. By accurately regulating the annealing temperature and holding time, micropores formed during sintering can be effectively eliminated, and residual stress can be released, therefore enhancing the metallurgical bonding strength between particles while improving surface finish and corrosion resistance[28–31]. However, the intrinsic relationship between structural evolution and property regulation in Fe-based bulk amorphous alloys during post-SPS annealing remains unclear, particularly regarding the synergistic optimization of mechanical properties and corrosion behavior.

In this research, Fe-based BMGs were synthesized using SPS. The effects of annealing treatment on the mechanical properties and corrosion resistance of these Fe-based BMGs were investigated. The complex yet intrinsic connection between the microstructural changes induced by annealing and the resultant property modifications was discussed. This research provided not only the structure-property relationship in Fe-based BMGs, but also a reliable foundation for the practical application of Fe-based BMGs across diverse industrial fields.

2 Experiment

FeCrMoBC[32] amorphous powder was used as the raw material. Through the gas atomization technique, this powder has an average particle size of 20 μm and a purity exceeding 99.5%. Table 1 presents the chemical composition of the FeCrMoBC Fe-based BMG. The powder sintering was conducted using an SPS-MKll 3.20 spark plasma sintering apparatus. In SPS experiment, a WC mold with a diameter of 12 mm was used, and the sintered samples had the dimensions of Φ12 mm×9 mm. The vacuum degree was set to 15 Pa, and the temperature was raised to the preset value at a heating rate of 100 °C/min. After holding at the target temperature for 1 min, the samples were cooled in argon gas with a cooling rate of 400 °C/min. Through the optimization of process parameters, FeCrMoBC BMGs were fabricated. Subsequently, heat treatment was performed on the as-sintered samples. The Fe-based BMGs were placed into tube-heating furnaces for annealing treatment under vacuum conditions at 500–650 °C for 20–80 min. Then, they were cooled to room temperature in the furnace.

The phase composition of the samples was analyzed by D/max-2400 X-ray diffractometer (XRD) with the scanning rate of 4°/min and the scan range of 20°–80°. The acquired data were processed by Jade software. The thermal characteristics of the amorphous powder were investigated using a PerkinElmer STA 6000 thermogravimetric-differential scanning calorimeter (TG-DSC). The measurements were conducted under a high-purity nitrogen atmosphere with the temperature ranging from 30 °C to 1000 °C at a heating rate of 20 °C/min. Microhardness measurements were performed using a WILSON VH1102 automatic microhardness tester, and the hardness scale was HV_1. Indentations were placed with an interval of 1 mm along the sample surface, and for each measurement, the results of 10 indentations were averaged. The compressive properties were evaluated on a YTP400-4E05A mechanical testing system at a strain rate of 1.4×10^{-4} s^{-1}. For the annealed Fe-based BMGs, corrosion tests were conducted in a 3.5wt% NaCl solution with a CHI600E electrochemical workstation. The surface and corrosion morphologies were observed using an FEI Quanta 450 FEG field-emission scanning electron microscope (SEM).

Table 1 Chemical composition of FeCrMoBC Fe-based amorphous powder (wt%)[32]

Fe	Cr	Mo	C	B
50.3–55.0	25.0–27.0	16.0–18.0	2.0–2.5	2.0–2.2

The densities of Fe-based BMGs were measured using Archimedes' method through the Shanghai Shunyu FA1004 electronic balance. The density (ρ_a) calculation formula is as follows:

$$\rho_a = \frac{m_1}{m_1 - m_2}\rho_w \quad (1)$$

where m_1 is the mass of the sintered sample measured in air (g), m_2 represents the mass of the sample fully immersed in deionized water (g), and ρ_w denotes the density of water at room temperature (0.9982 g/cm^3). This method accounts for buoyancy effects by measuring the apparent mass loss of the sample in water, enabling precise determination of its actual density through volume displacement calculations.

The theoretical density of the Fe-based BMG was determined via the rule of mixtures, which can be calculated using the following formula:

$$\rho_d = \frac{1}{\frac{a}{\rho_{Fe}} + \frac{b}{\rho_{Cr}} + \frac{c}{\rho_{Mo}} + \frac{d}{\rho_C} + \frac{e}{\rho_B}} \quad (2)$$

where a, b, c, d, and e represent the content of elements Fe, Cr, Mo, C, and B in Fe-based BMG, respectively (wt%); ρ_{Fe}, ρ_{Cr}, ρ_{Mo}, ρ_C, and ρ_B are used to denote the theoretical density of the elements Fe, Cr, Mo, C, and B, respectively (g/cm^3).

3 Results and Discussion

3.1 Characteristics of Fe-based amorphous powders

Fig. 1a presents XRD pattern of the Fe-based amorphous powder. A characteristic diffraction peak corresponding to amorphous state is observed at 2θ=40°–50°, indicating the fully amorphous nature of the fabricated FeCrMoBC powder. Fig. 1b presents SEM image of the Fe-based amorphous powder, showing that the aerosolized FeCrMoBC amorphous powder exhibits a typical spherical morphology. The particle sizes are centered at 20 μm, and no obvious defects can be observed on the smooth particle surface.

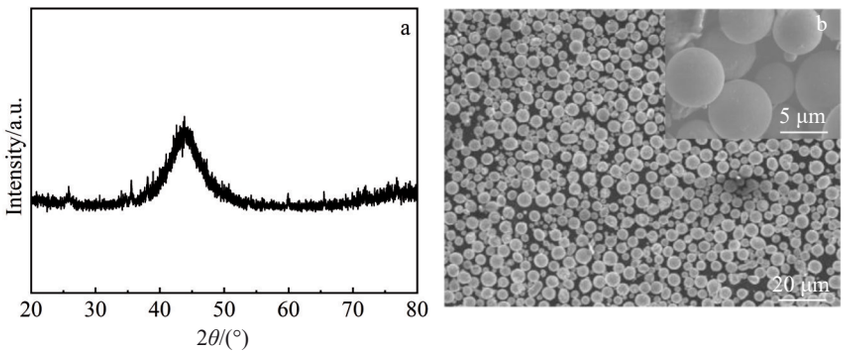

Fig.1 XRD pattern (a) and SEM image (b) of Fe-based amorphous powder[32]

3.2 Fe-based BMGs fabricated by SPS

According to Ref. [33], the optimized sintering parameters were determined as follows: sintering temperature ranging from 500 °C to 600 °C, sintering pressure of 550 MPa, heating rate of 100 °C/min, and holding time of 1 min. The relatively high sintering pressure of 550 MPa not only promotes the densification of BMG, but also effectively inhibits the formation of fully crystalline phases or coarse grains.

Fig. 2a displays XRD patterns of the FeCrMoBC samples after SPS at different temperatures. It can be seen that XRD patterns of the samples after SPS at 500 – 560 °C closely resemble those of the amorphous powder: no crystalline diffraction peaks can be observed. This result indicates that these BMGs can maintain their amorphous structure under the temperatures of 500–560 °C. However, when the temperature reaches 600 °C, the intensity of the diffraction peak corresponding to amorphous structure decreases significantly, suggesting the initiation of crystalline phase precipitation within the amorphous matrix. Fig. 2b shows the relative density curves of the FeCrMoBC samples after SPS at different temperatures. It can be seen that the relative density is increased steadily with the increase in SPS temperature, achieving a maximum value of 94.40% at 560 °C. In conjunction with XRD results in Fig. 2a, it can be concluded that SPS at this temperature (560 °C) barely changes the amorphous structure. Consequently, the optimal SPS parameters are obtained: temperature of 560 °C, consolidation pressure of 550 MPa, heating rate of 100 °C/min, and holding time of 1 min. The sample prepared by SPS under these conditions is designated as 1#.

Fig. 3 shows SEM images of sample 1#. The amorphous powder particles undergo significant deformation and are transformed from their initial spherical morphology to irregular polyhedral structures, as indicated in Fig. 3b. This morphological evolution indicates effective interfacial diffusion and fusion between particles during high-pressure (550 MPa) SPS. Notably, metallurgical bonding interfaces are formed between particles, and no pores or crack defects can be observed. This phenomenon is consistent with the findings in Ref. [34]. These experiment results confirm that the Fe-based BMG fabricated via this process exhibits high densification and retains its amorphous state, providing a solid foundation for subsequent heat treatment.

3.3 Mechanical properties of heat-treated (annealed) samples

To investigate the influence of heat treatment (annealing) on the performance of SPSed samples, a comprehensive thermodynamic analysis was conducted on sample 1# to provide theoretical guidance for subsequent optimization of heat treatment process. Fig. 4 presents DSC curve of sample 1#, revealing a glass transition temperature (T_g) of 610 °C, an onset crystallization temperature (T_x) of 665 °C, and a corresponding supercooled liquid region width ($\Delta T_x=T_x - T_g$) of 55 °C. The broad supercooled liquid region indicates excellent thermal stability of sample 1#, which is highly favorable for subsequent annealing of Fe-based BMG[35]. Based on this analysis, the annealing temperatures were selected below T_g to prevent unintended crystallization caused by excessive

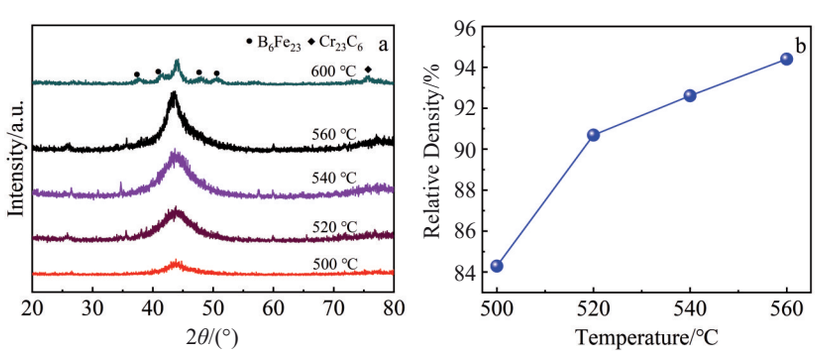

Fig.2 XRD patterns (a) and relative densities (b) of FeCrMoBC samples after SPS at different temperatures

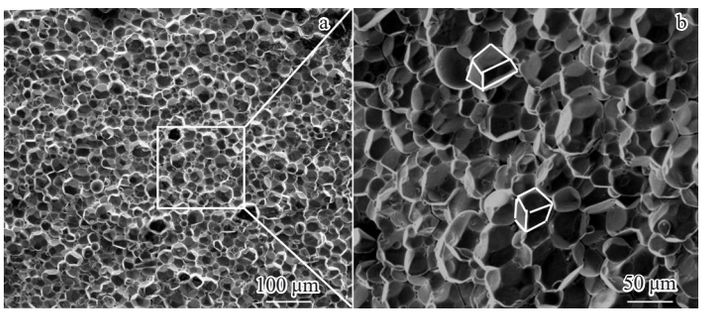

Fig.3 SEM images of sample 1#

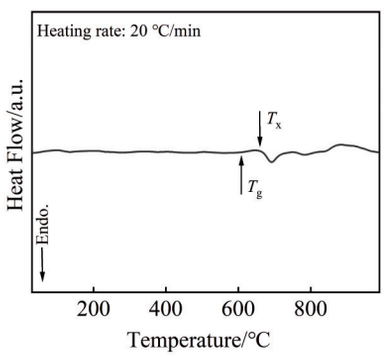

Fig.4 TG-DSC curve of sample 1#

thermal energy[36–37]. A series of annealing treatments with optimized parameters were then performed on sample 1#, as listed in Table 2.

Fig.5a shows XRD patterns of sample 1# after annealing at various temperatures. It can be seen that the diffraction peaks of samples 1-1# and 1-2# are slightly narrower than those of sample 1#, indicating that samples 1-1# and 1-2# still maintain the amorphous structure. Samples 1-3# and 1-4# exhibit significantly increased crystallinity, accompanied by the precipitation of FeC, B_6Fe_{23}, and $Cr_{23}C_6$ crystalline phases. The emergence of the Fe_2MoB_4 phase in sample 1-4# indicates a substantial increase in crystallinity, compared with that of sample 1#. Crystallization becomes more pronounced with the increase in annealing temperature, due to the enhanced atomic diffusion that promotes grain nucleation, growth, and phase precipitation. Fig.5b displays XRD patterns of sample 1# after annealing for different durations. With the prolongation of holding time, diffraction peaks are progressively sharpened, and the crystalline phase precipitation becomes more prominent. These results indicate that crystallinity is increased with the prolongation of holding time.

Table 2 Annealing process parameters of sample 1#

Sample	Annealing temperature/°C	Holding time/min	Heating rate/°C·min^{-1}
1-1#	500	20	10
1-2#	550	20	10
1-3#	600	20	10
1-4#	650	20	10
1-5#	550	50	10
1-6#	550	80	10

Fig. 6a illustrates the effect of annealing temperature on microhardness of Fe-based BMG samples. Compared with sample 1#, other samples demonstrate a general downward trend in microhardness. This variation is consistent with the phenomena of narrowing of diffraction peaks and emergence of crystalline diffraction peaks associated with phase precipitation. Besides, the distinct non-uniform hardness distribution can be characterized by central regions of higher hardness and marginal zones of lower hardness. This result is consistent with the edge effects reported in Ref.[38]. When the annealing temperature increases from 500 °C (sample 1-1#) to 650 °C (sample 1-4#), the average microhardness rises significantly from 604.41 HV to 758.86 HV. This increase is primarily due to the enhanced nucleation of precipitate phases at elevated temperatures, which restricts shear band propagation through dispersion strengthening mechanisms. Conversely, Fig. 6b shows that the microhardness evolution

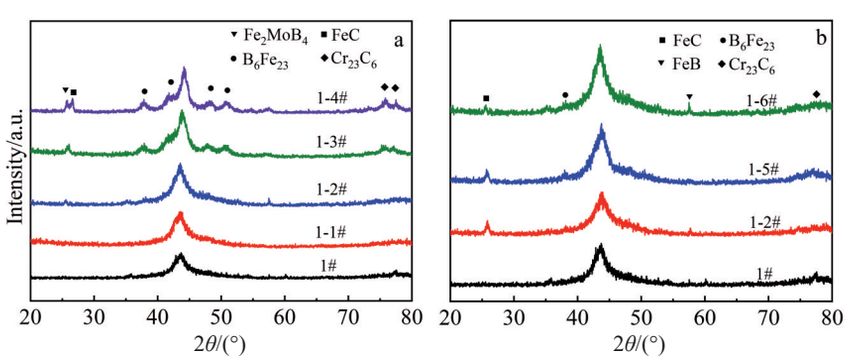

Fig.5 XRD patterns of sample 1# after annealing under different temperatures (a) and different holding time (b)

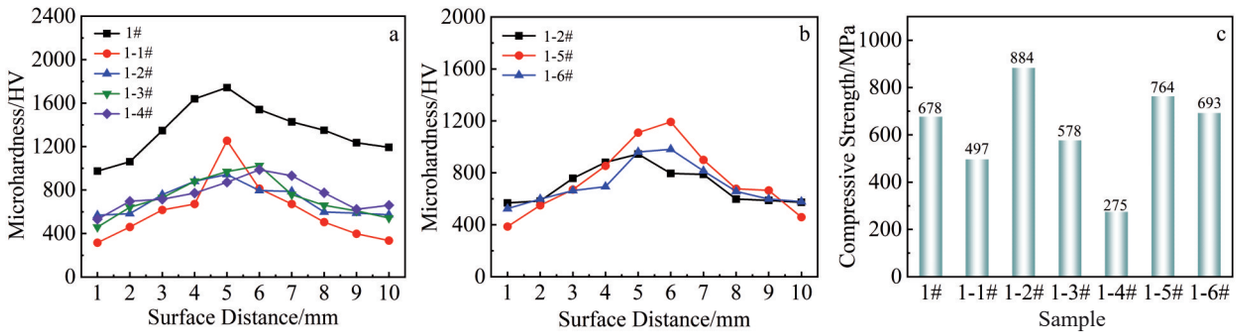

Fig.6 Effects of annealing temperature (a) and holding time (b) on microhardness of Fe-based BMG samples; comparison of compressive strength of Fe-based BMG samples (c)

during isothermal annealing follows a parabolic trend: the microhardness initially increases, reaches a maximum value of 746.49 HV (50 min, sample 1-5#), and then decreases. The peak-hardening behavior occurs at 50 min. This phenomenon can be explained by the optimal precipitate distribution, while the subsequent microhardness reduction beyond 50 min is attributed to the precipitate coarsening, which weakens the dispersion strengthening effect. Notably, the sample 1-5# (annealing for 50 min) exhibits significantly higher microhardness, compared with either sample 1-2# (annealing for 20 min) and sample 1-6# (annealing for 80 min), highlighting the critical role of time-temperature interplay in microstructure-property relationships.

Fig. 6c shows the compressive strength of the Fe-based BMG samples. The compressive strength of samples 1-2#, 1-5#, and 1-6# is all greater than that of sample 1#. This enhancement can be ascribed to the improved particle bonding and the reduced porosity during the heat treatment process. Nonetheless, the further increase in annealing temperature results in a notable decline in compressive strength. This is presumably because of the extensive precipitation of crystalline phases, along with the formation of quenched nuclei or the initiation of crystalline phase nucleation, which in turn leads to the embrittlement of the matrix. Under the condition of annealing temperature at 550 °C, the compressive strength of sample 1-2# reaches the peak value of 884 MPa. Under the same annealing temperature, with the prolongation of holding time to 80 min, the compressive strength is gradually decreased to 693 MPa (sample 1-6#). These findings suggest that the optimal annealing parameters are as follows: annealing temperature of 550 °C and holding time of 20 min.

Fig. 7 presents SEM surface morphologies and relative density of different Fe-based BMG samples. Sample 1# illustrates a granular morphology with surface particles loosely packed without significant interparticle fusion, which is manifested as weak interparticle bonding. Annealing induces significant morphological changes: partial particle melting and fusion can be observed with the increase in annealing temperature, which enhances the interparticle bonding. At higher temperatures, particles can form not only stronger connections but also develop lamellar planar structures, leading to multiplanar interlocking. This phenomenon is likely attributed to the elevated temperatures that promote the particle mobility and facilitate the atomic diffusion for fusion. Fig. 7h displays the relative density of different Fe-based BMG samples. A marked increase in relative density can be observed after annealing: the relative density is generally increased with the increase in annealing temperature or with the prolongation of holding time. Notably, prolonged holding time has a less pronounced effect on relative density, compared with annealing temperature. In the initial annealing stage, increased annealing temperature and prolonged holding time both promote the particle rearrangement, diffusion, and flow, thereby reducing porosity and enhancing densification. However, prolonged holding time at elevated temperatures leads to recrystallization and increased crystallinity, which further hinders the relative density increase due to reduced atomic mobility and pore closure efficiency. Thus, when the FeCrMoBC BMG is annealed at 650 °C for 20 min, the relative density is 97.23%, and the microhardness is 758.86 HV.

3.4 Corrosion properties of heat-treated (annealed) samples

Fig. 8a shows Tafel curves of Fe-based BMG samples during corrosion in 3.5wt% NaCl solution. Combined with the potentiodynamic polarization parameters in Table 3, it can be seen that the corrosion potential (E_{corr}) generally shows a decreasing trend, while the corresponding corrosion current density (I_{corr}) shows an increasing trend, indicating that the corrosion rate of the annealed samples increases, and the corrosion resistance gradually deteriorates. With the increase in annealing temperature, the corrosion resistance is firstly increased and then decreased. This is because when the annealing temperature is low in the early stage, the samples basically maintain the amorphous state, and the relative density is increased with the increase in annealing temperature, thus improving the corrosion resistance. As the annealing temperature continues to rise, although the relative density still increases, the increment is small and basically remains a gentle growth state, while the degree of crystallization is increased exponentially. In this case, a large number of crystalline phases appear, leading to the deterioration of corrosion resistance. For sample 1-2#

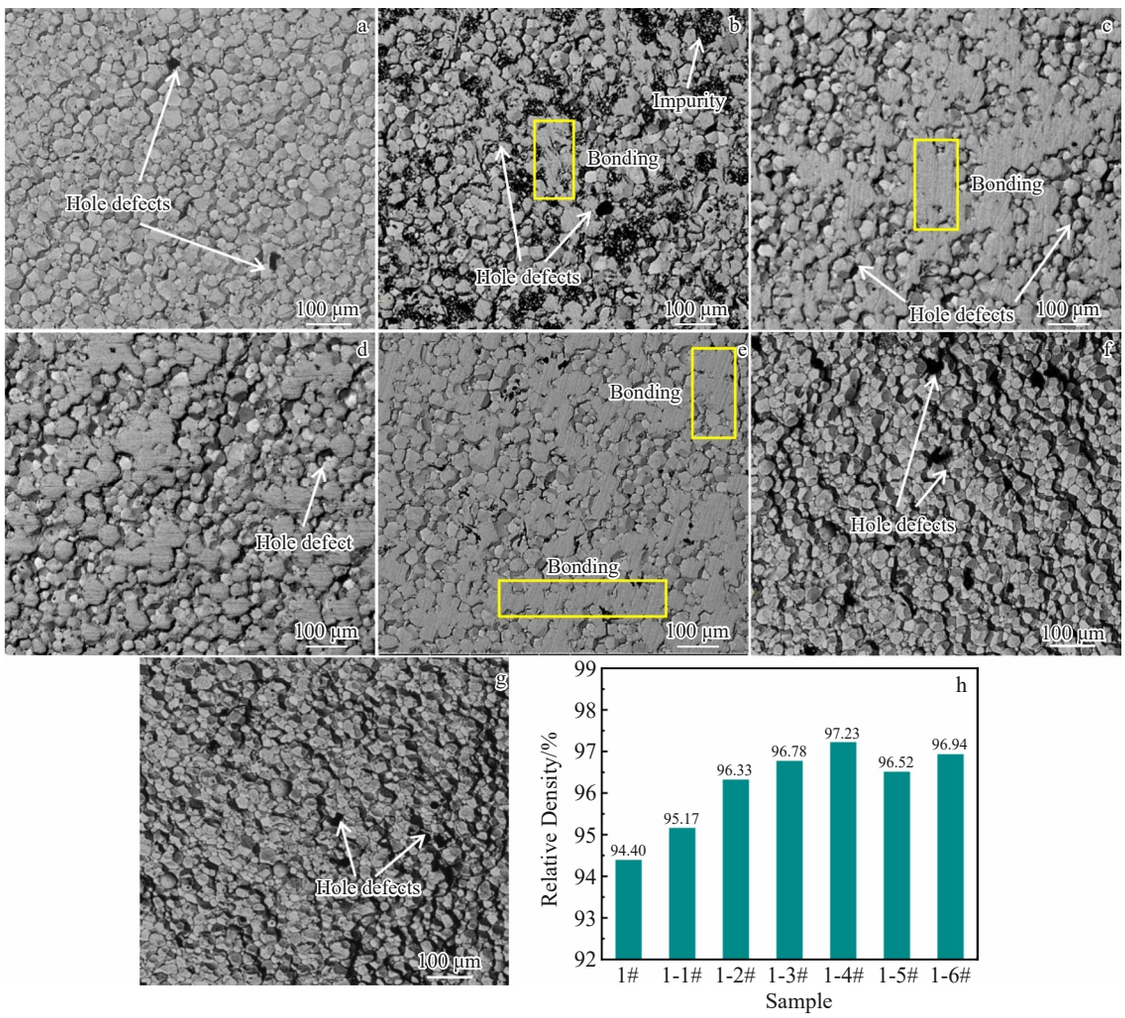

Fig.7 SEM surface morphologies (a–g) and relative density (h) of Fe-based BMG samples: (b) 1#; (b) 1-1#; (c) 1-2#; (d) 1-3#; (e) 1-4#; (f) 1-5#; (g) 1-6#

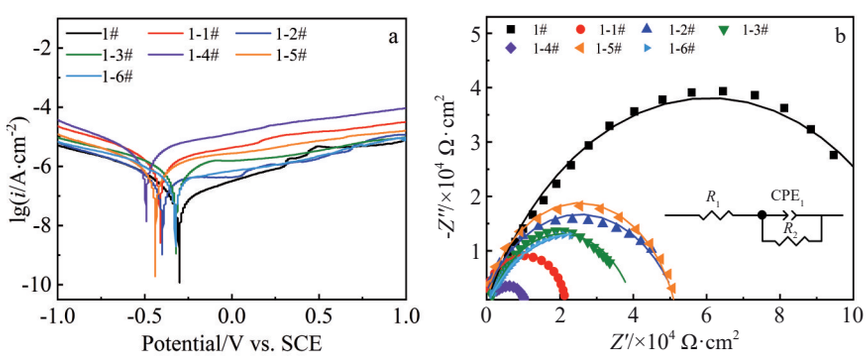

Fig.8 Tafel curves of Fe-based BMG samples in 3.5wt% NaCl solution (a); Nyquist plots and equivalent circuit diagram of Fe-based BMG samples (b)

(annealing at 550 °C), its E_{corr} reaches the maximum value of −0.318 V, and its I_{corr} reaches the minimum value of 2.098×10^{-7} A/cm^2, indicating that the corrosion resistance is optimal. Meanwhile, electrochemical test results show that with the prolongation of holding time, E_{corr} is decreased and I_{corr} is increased, indicating that the corrosion resistance shows a decreasing trend. In conclusion, the sample 1-2# has the optimal corrosion resistance.

Fig. 8b shows the Nyquist plots of the Fe-based BMG samples during corrosion in 3.5wt% NaCl solution. It is known that the larger the arc diameter, the slower the corrosion rate. The corrosion resistance of sample 1# is better than that of other samples. This may be due to the severe crystallization of the samples after heat treatment: the diffraction peaks become sharp, accompanied by the appearance of defects, such as crystalline phases that are

prone to corrosion[39–40]. With the increase in annealing temperature, the corrosion resistance is firstly improved and then degraded, while the prolongation of holding time degrades the corrosion resistance. The impedance data were fitted using Z-View software based on the equivalent circuit model (inset in Fig. 8b), and the equivalent circuit parameters are obtained, as shown in Table 3. The charge transfer resistance (R_2) is proportional to the corrosion resistance. Therefore, it is found that the change in R_2 is consistent with the analysis results: the corrosion resistance is firstly improved and then degraded with the increase in annealing temperature. For sample 1-2# (annealing temperature of 550 °C), R_2 reaches the maximum value of 59 379 Ω·cm^2. Besides, with the fixed annealing temperature (550 °C), the corrosion resistance is degraded with the prolongation of holding time. In conclusion, the sample 1-2# has excellent corrosion resistance.

Fig. 9 shows SEM images of different Fe-based BMG samples after corrosion in 3.5wt% NaCl solution. It can be seen that the corrosion trace of sample 1# is generally smaller than that of other samples, indicating better corrosion resistance of sample 1#. As the annealing temperature increases (Fig. 9b – 9e), the corrosion traces show a trend of first decrease and then increase. When the annealing temperature is 500 °C, the sample 1-1# remains the amorphous state, its relative density is low, and many pores exist in

Table 3 Electrochemical parameters of Fe-based BMG samples

Sample	E_{corr}/V	I_{corr}/A·cm^{-2}	R_1/Ω·cm^2	CPE$_1$-T/μF·cm^{-2}	CPE$_1$-P/μF·cm^{-2}	R_2/Ω·cm^2	χ^2
1#	−0.249	2.359×10^{-8}	3 867.0	4.095×10^{-9}	0.802 92	129 090	2.1×10^{-3}
1-1#	−0.412	7.739×10^{-7}	903.6	4.699×10^{-10}	0.984 79	22 568	6.2×10^{-4}
1-2#	−0.318	2.098×10^{-7}	4 333.0	1.097×10^{-9}	0.933 07	59 379	3.7×10^{-3}
1-3#	−0.436	3.339×10^{-7}	839.5	2.734×10^{-8}	0.749 01	39 807	2.4×10^{-3}
1-4#	−0.493	1.387×10^{-6}	652.0	9.686×10^{-9}	0.765 86	10 141	9.9×10^{-4}
1-5#	−0.324	4.386×10^{-7}	2 186.0	3.007×10^{-10}	0.985 61	54 880	7.1×10^{-4}
1-6#	−0.397	3.534×10^{-7}	197.3	7.785×10^{-8}	0.646 78	47 060	2.8×10^{-5}

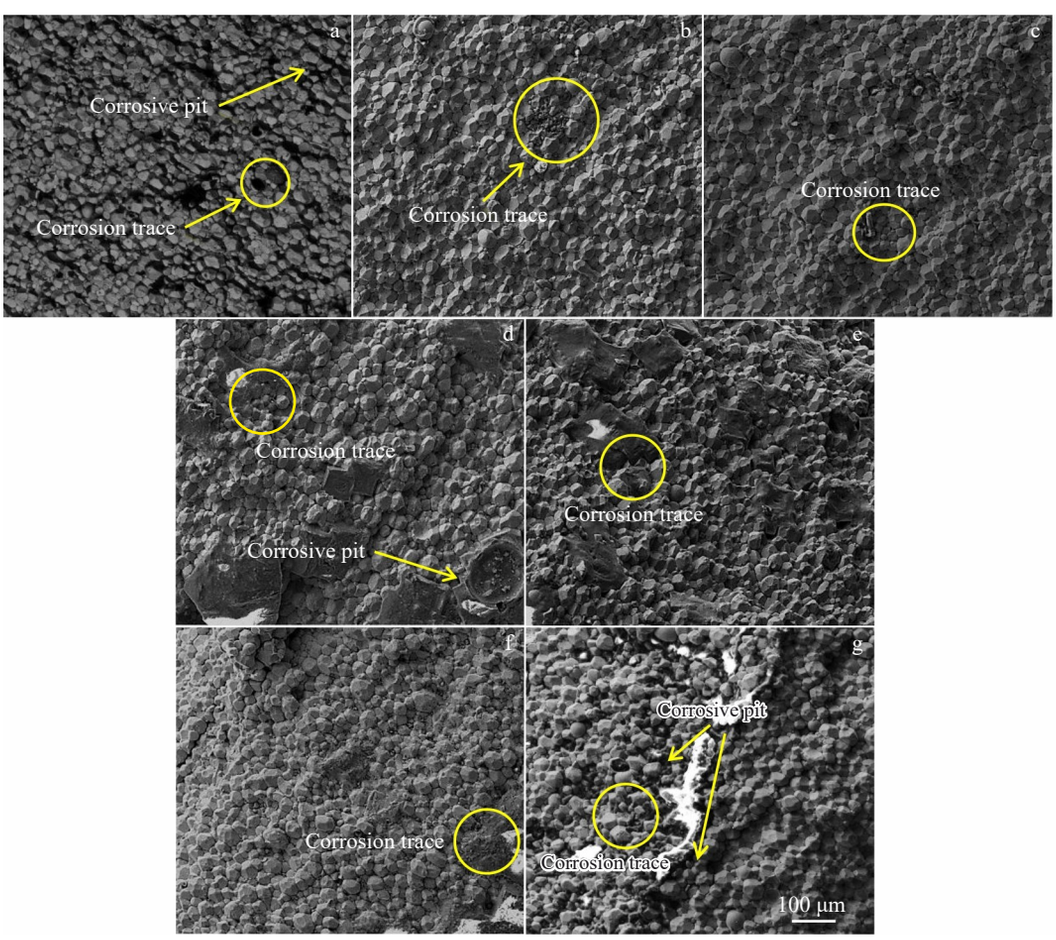

Fig.9 SEM images of different Fe-based BMG samples after corrosion in 3.5wt% NaCl solution: (a) 1#; (b) 1-1#; (c) 1-2#; (d) 1-3#; (e) 1-4#; (f) 1-5#; (g) 1-6#

the sample. Many Cl^- ions invade, and corrosion channels are formed, resulting in inferior corrosion resistance. When the annealing temperature reaches 550 °C, the sample 1-2# is still amorphous, but its relative density significantly increases, and the defects, such as pores, greatly reduce. In this case, the corrosion resistance reaches the optimal state. With the further increase in annealing temperature, a large number of crystalline phases are precipitated and preferentially corroded, leading to the appearance of dense corrosion pits or even large-area corrosion traces on the sample surface. Thus, the corrosion resistance deteriorates. With the fixed annealing temperature of 550 °C (Fig. 9c, 9f, 9g), the corrosion traces show an increasing trend with the prolongation of holding time, but the overall increase trend is insignificant. This result indicates that the influence of holding time on the corrosion resistance is slighter than that of annealing temperature. Among all the samples, the sample 1-2# has the optimal corrosion resistance.

4 Conclusions

1) Fully dense FeCrMoBC BMGs can be fabricated under optimized processing parameters of SPS temperature of 560 °C, consolidation pressure of 550 MPa, and holding time of 1 min. This processing window yields BMG with a relative density of 94.40%, representing a significant improvement in relative density.

2) After annealing treatment, the degree of crystallization in FeCrMoBC BMG increases, accompanied by the rise in densification. Additionally, the bonding is strengthened, and the porosity is reduced.

3) The compressive strength reaches the highest value of 884 MPa when the annealing temperature is 550 °C and the holding time is 20 min. Corrosion resistance also achieves the optimal state: E_{corr} reaches the highest value of −0.318 V, I_{corr} reaches the lowest value of 2.098×10^{-7} A/cm^2, and R_2 reaches the highest value of 59 379 Ω·cm^2. When the FeCrMoBC BMG is annealed at 650 °C for 20 min, the relative density is 97.23%, and the microhardness is 758.86 HV.

References

1 Wang Y, Xing Z, Luo Q *et al. Corrosion Science*[J], 2015, 98: 339

2 Cukic B, Mitrovic N, Maricic A. *China Foundry*[J], 2017, 14(1): 59

3 Nayak S K, Anil K, Tapas L. *International Materials Reviews*[J], 2023, 68(4): 404

4 Li Y C, Zhang W W, Wang Y *et al. Surface & Coatings Technology*[J], 2022, 437: 128377

5 Dong Q S, Zhang B S, Ba Z X *et al. Surface Topography: Metrology and Properties*[J], 2019, 7(4): 044001

6 Zeng Q S, Sheng H W, Ding Y *et al. Science*[J], 2011, 332(6036): 1401

7 Cheng Y Q, Ma E. *Progress in Materials Science*[J], 2011, 56: 379

8 Wang L, Wang J G, Sun M T. *Chemical Physics Letters*[J], 2020, 750: 137511

9 Xu D D, Zhou B L, Wang Q Q *et al. Corrosion Science*[J], 2018, 138: 20

10 Fan Y Z, Zhang S, Xu X F *et al. Intermetallics*[J], 2021, 138: 107306

11 Inoue A, Kong F L, Man Q K *et al. Journal of Alloys and Compounds*[J], 2014, 615(S1): S2

12 Li F C, Liu T, Zhang J Y *et al. Materials Today Advances*[J], 2019, 4: 100027

13 Xie G Q, Ohashi O, Yoshioka T *et al. Materials Transactions*[J], 2001, 42(9): 1846

14 Xie G Q, Ohashi O, Yamaguchi N *et al. Metallurgical & Materials Transactions A*[J], 2003, 34(11): 2655

15 Ding H P, Bao X Q, Zhang M *et al. Advanced Powder Materials*[J], 2023, 2(3): 100109

16 Ding H P, Zhao Z K, Jin J S *et al. Journal of Alloys and Compounds*[J], 2021, 850: 145726

17 Yang C, Zhu M D, Luo X *et al. Scripta Materialia*[J], 2017, 139: 96

18 Li X X, Yang C, Liu Z *et al. JOM*[J], 2019, 71(8): 2475

19 Saijyothi N, Arvindha D B, Srinivasarao B *et al. Journal of Alloys and Compounds*[J], 2021, 876: 160057

20 Li X X, Yang C, Chen T *et al. Journal of Alloys and Compounds*[J], 2019, 802: 600

21 Liu M J, Xu L J, Li Z *et al. Rare Metal Materials and Engineering*[J], 2024, 53(5): 1236

22 Ratzker B, Sokol M. *Materials & Design*[J], 2023, 233: 112238

23 Kelly J P, Fuller S M, Seo K *et al. Materials & Design*[J], 2016, 9: 26

24 Harimkar S P, Paital S R, Singh A *et al. Journal of Non-Crystalline Solids*[J], 2009, 355: 2179

25 Ding H P, Zhao Z K, Jin J S *et al. Journal of Alloys and Compounds*[J], 2020, 850: 156724

26 Tan Z, Wang L, Xue Y F *et al. Materials Science & Engineering A*[J], 2015, 642: 377

27 Graeve O A, Saterlie M S, Kanakala R *et al*. *Scripta Materialia*[J], 2013, 69: 143

28 Zhang W F, Meng Y, Wang J F *et al*. *Materials Letters*[J], 2022, 15: 315

29 Prater J T, Merz M D. *Journal of Applied Physics*[J], 1981, 52(3): 1877

30 Yang Y Z, Mao J, Zhao D Q *et al*. *Heat Treatment of Metals*[J], 2006, 31(1): 3

31 Zhou S F, Xu Y B, Liao B Q *et al. Optics and Laser Technology*[J], 2018, 103: 8

32 Li C Y, Wang H B, Ding J Q *et al. Materials Science and Technology*[J], 2020, 37(5): 2168

33 Li C Y, Chen J X, Hou S J *et al. Materials Today Communications*[J], 2023, 37: 107068

34 He G M, Chen Q J. *Journal of Alloys and Compounds*[J], 2019, 797: 213

35 Wang X H, Wang G, Zhu Y Y *et al. Transactions of Nonferrous Metals Society of China*[J], 2014, 24(3): 712
36 Roy D, Singh S S, Basu B *et al. Wear*[J], 2009, 266(1–2): 1113
37 Murali P, Ramamurty U. *Acta Materialia*[J], 2005, 53: 1467
38 Fu B Y, He D Y, Zhao L D. *Journal of Alloys and Compounds*[J], 2009, 480: 422
39 Zhou Y T, Wang T. *Journal of Materials Research and Technology*[J], 2024, 30: 256
40 Li L D, Lin B, Zhang H L *et al. ACS Sustainable Chemistry & Engineering*[J], 2024, 12(39): 14425

放电等离子烧结Fe基块体非晶合金中退火诱导的力学强度与耐腐蚀性能提升

李春燕[1,2,3]，刘建辉[2]，高嘉庆[2]，陈佳欣[2]，权国宁[2]，张　强[2]，寇生中[1,2,3]，李晓诚[1,2]
(1. 兰州理工大学 省部共建有色金属先进加工与再利用国家重点实验室，甘肃 兰州 730050)
(2. 兰州理工大学 材料科学与工程学院，甘肃 兰州 730050)
(3. 兰州理工大学 温州泵阀工程研究院，浙江 温州 325105)

摘　要：通过放电等离子烧结（SPS）技术制备FeCrMoBC系块体非晶合金，并采用后续热处理优化其性能，探究了退火处理对Fe基块体非晶合金显微组织、力学行为及耐腐蚀性能的影响。结果表明：在优化SPS工艺参数（烧结温度560 ℃、烧结压力550 MPa、保温时间1 min）后，烧结态试样的相对密度达94.40%，抗压缩强度为678 MPa；经550 ℃×20 min热处理后，试样仍保持非晶态结构，力学性能显著提升——抗压缩强度增至884 MPa，同时展现出优异的耐腐蚀性能，其开路电位（E_{corr}）为−0.318 V、腐蚀电流密度（I_{corr}）为2.098×10^{-7} A/cm^2、极化电阻（R_2）为59 379 Ω·cm^2。值得注意的是，经650 ℃×20 min退火处理后，试样因晶相析出与晶粒细化，相对密度达到最大值97.23%，显微硬度也升至峰值758.86 HV。上述结果表明，通过调控显微组织演化，可控热处理可有效改善SPS制备Fe基块体非晶合金的致密化程度与综合性能。

关键词：SPS技术；Fe基块体非晶合金；热处理；力学行为；耐腐蚀性能

作者简介：李春燕，女，1979年生，博士，教授，兰州理工大学省部共建有色金属先进加工与再利用国家重点实验室，甘肃 兰州 730050，E-mail：lichunyan@lut.edu.com